Gems & Gemology

WINTER 1975-1976

RICHARD T. LIDDICOAT, JR.
Editor

ROBERT A. P. GAAL, Ph.D.
Assoc. Editor

ISSN 0016-62X

Gems & Gemology

VOLUME XV NUMBER 4

WINTER 1975-1976

IN THIS ISSUE

The Variable Effects of Faceted Gemstones

BY WERNER R. EULITZ, Ph.D.
Huntsville, Alabama

Summary

The external appearance of a faceted gemstone is based upon internal double-reflections at the pavilion facets. The mechanism of internal double-reflection can be described by a simple optical law in which the facet angles are independent variables. The transparency and the refractive index of the gem material reduce the reflectivity of the pavilion and the escape of reflected light through the crown facets.

The limitations of reflectivity through the table and through the crown facets are depicted in diagrams for varying pavilion- and crown facet-angles of several stone materials. The charts provide the basis to analyze the external appearance of any cut.

Comparison of "historical cuts," advocated by H. Tillander, Finland, with the standard brilliant-cut diamond shows that the historical cuts, indeed, provide high brilliancy plus dispersion, while the standard brilliant is primarily designed for optimum brilliancy. With a slight modification of crown facet angles, however, the dispersion effect and so the total appearance of the standard cut can be made superior to the historical cuts.

1. Introduction

The most popular type of faceted gemstones is the round-cut, a simulation of the brilliant-cut diamond. Other forms, such as the emerald-cut, the octagon, the square cut, etc., may be considered modifications of the round-cut by stretching some facet arrangements lengthwise and reducing or eliminating others. All these cuts, applied mostly to transparent stones, have in common a lower faceted portion, the pavilion, and an upper portion, the crown, which are geometrically separated by an imaginary girdle plane.

Transparent colored stones are being faceted to emphasize the beauty of their color; transparent colorless stones, which will be considered in the following only, are being faceted for brilliance and dispersion. The latter two phenomena have been subject to numerous investigations for many years, especially on diamond.

Brilliance is characterized by the strong metallic internal reflections of the pavilion facets; dispersion, in gemology called the fire, is the resolution of the different wavelengths of white light into the popular rainbow colors (spectrum).

For optimum brilliance, a standard brilliant has been developed over many years. This standard design has been the subject of several criticisms in recent publications, especially by Tillander, Finland, and others, for its lack of strong dispersion effects. This controversy stimulated the following investigation on the variability of optical effects by different facet angles.

The mathematical treatment of the problem is not in great esteem even among experts, although it is obvious that a faceted gemstone is an optical device like a lens or a mirror system, the quality of which is always correlated to strong optical laws. The optical effects of faceted gemstones depend on relatively simple laws. It will be shown in the following discussions that many prevailing arguments can be resolved and new design criteria can be discovered by proper interpretation of the optical laws involved.

2. Refraction

Light travels with a velocity (Light Velocity = LV) which is a maximum in vacuum. In air, the LV is only slightly less than in vacuum so that for practical purposes, the LV in air is commonly used for reference. When a light ray enters a stone, its velocity is reduced by a factor "n". This means, expressed by a simple formulation,

$$LV\ (air) = n \bullet LV\ (stone)$$

The factor "n" is called the refractive index of the stone material.

The reduction of LV inside a stone causes a change of the direction of a ray entering the stone. This change of direction at the boundary between the two media is called "refraction." The degree of refraction depends on the size of the angle of an entering ray in air which always, as any light ray angle, is measured with respect to the normal (a line NN vertical to the surface at the point of incidence). The angle of the ray inside the stone is smaller than the angle in air. It has been discerned that the ratio of the trigonometrical sine-functions (abbreviated "sin") of the two angles is always equal to the refractive index "n". Thus,

$$\frac{\sin\ (\text{angle in air})}{\sin\ (\text{angle in stone})} = n$$

This is Snell's law of refraction which can be solved graphically as demonstrated and explained in *Figure 1.* The application of this method is presented in *Figure 2* for diamond, zircon, corundum, and quartz.

The scale divisions of the stone-scales *(Figure 2)* increase rapidly from about 45° (in air) upward. In diamond, up to 60° in air are distributed inside the stone to about 20°, while the remaining 30° in air are spread over 4° only, inside the stone.

The refractive indices for violet and red light in diamond are considerably different. In *Figure 2*, the diamond circle is referred to violet light (n = 2.45). For red light (n = 2.41) the circle would be larger. It is drawn for a short distance. Thus, from a white light ray striking a face inside the stone under an angle of 24° (diamond scale), the violet ray will go to the outside with an angle of 90° (air scale). However, the 24°-vertical line intersects the red light circle at point P. Consequently, the red light will depart the stone with an angle of about 77.5° (line from point C over P to the air scale). This means the original white light ray is dispersed into the spectrum with an angular margin of about 12°. This angular margin obtained from *Figure 2* is in absolute agreement with earlier, very accurate physical measurements. It also follows from the diagram of *Figure 2* that the dispersion in the lower degree bracket is negligible.

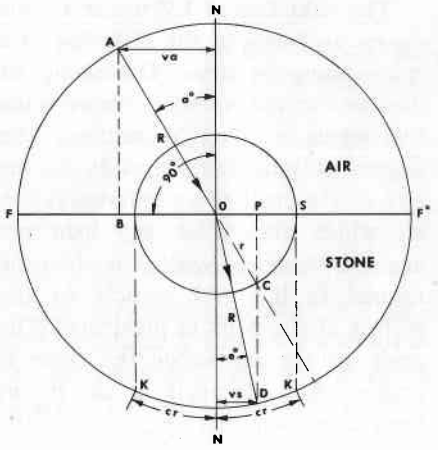

Fig. 1. Graphical Solution of Snell's Law of Refraction.
The refractive index n of a gemstone is the proportionality factor between the light velocity (LV) in air (vacuum) and in the stone, so that

$$\frac{LV\ (air)}{LV\ (stone)} = n$$

Assume n = 2.5, line FOF a facet of the stone, and FO = AO = R the LV(air), then, OS = OC = r = R/2.5 is the LV(stone). Ray AO impinges on the facet FF* at point O under an angle of incidence (a). The extension of ray AO intersects the stone circle r at point C. The velocity component of AO is BO = va in air, and OP = vs in the stone, va : vs = n = 2.5. The ray in the stone arrives at point D under an entering angle (e); e < a. Ratio va:R = sin (a); and vs:R = sin (e). Thus, va:vs = n = sin (a)/sin (e). This is Snell's law of refraction. It applies only to rays passing from one medium into another one (air – stone, or reverse). The light path inside the stone is unaffected by this law.*

In *Figure 1*, only one ray is indicated. Within the same plane of incidence (drawing plane), a similar ray from the right side of the normal NN is possible also. The angle of incidence in air can be decreased to 90° at both sides of the normal; inside the stone, however, the angle for diamond can only increase to 24°, also at both sides of the normal. Thus, from the outside, rays of any incident angle can enter the stone within a margin of 180°. Inside a diamond, the angular margin is only 48° (2 x 24°). Since the path of a light ray is reversible, only rays striking a facet from inside the stone with an angle smaller than 24° (diamond) can escape to the outside; all other rays are reflected back into the stone. This is the critical angle cr = 24° for diamond.

Reflections inside a stone by rays striking a facet from the inside with an angle larger than the critical angle are called "total" reflections. They obey a simple law which states that the angle

of incidence is equal to the angle of reflection; the angles again measured with respect to the normal.

3. The Light Path Inside the Stone

In order to reflect the entering light rays back toward the observer, the rays are usually reflected twice inside the stone. This is accomplished by two opposite pavilion facets which are arranged symmetrically to the center line of the stone and perpendicular to the plane of incidence (drawing plane). Due to this arrangement, the path of a light ray inside the stone is divided into three distinct sections. Each section forms a triangle with the facets being touched. A ray entering the stone at point A, *Figure 3,* with an angle "e", arrives at the pavilion facet at point B with an angle "x_1", with respect to the normal. It is reflected with the same angle "x_1" (law of reflection) to the opposite pavilion

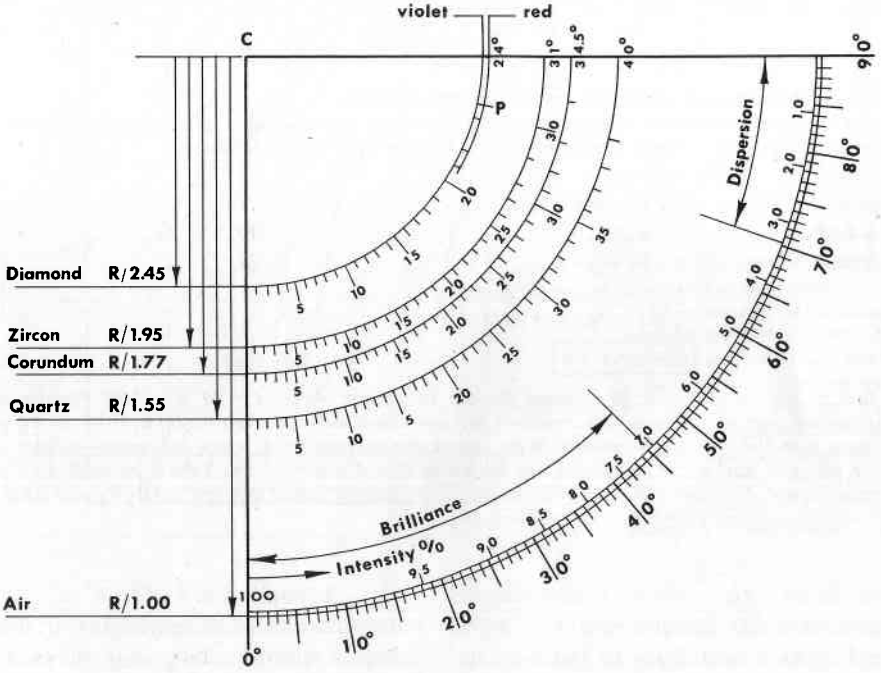

Fig. 2. Nomograph to determine angles of refraction (Snell's Law).
This diagram is designed for practical usage, based on the principle described in Fig. 1. The air scale (outer circle) is linear. The scales of the stone circles (non-linear) are obtained by projecting the angles of the air scale parallel to line CO upward to the stone circles, similar to lines DP and KS in Fig. 1. To find the refractive angle inside a stone of a ray impinging the facet with an angle of 50° in air, for example, connect point C with the 50°-point at the air scale. Then, the refractive angle for diamond is approximately 18°, for zircon 23°, for corundum 25°, and for quartz 30°. The procedure is reversible. A ray coming from the inside with an angle of 15°, would emerge in air with an angle for diamond 39°, zircon 30°, corundum 27°, and quartz 23°.

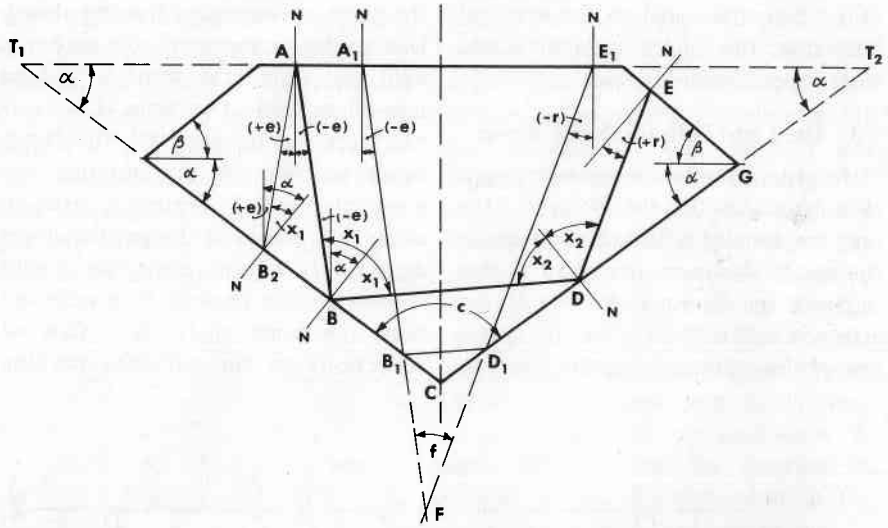

Fig. 3. Derivation of the law of internal double reflection.
The light path inside the stone is divided in 3 sections due to double reflection. Each section forms a triangle (Δ) with the facets touched by the light ray. It follows,

ΔBDC: $(90^\circ - x_1) + (90^\circ - x_2) + c = 180^\circ$

thus, $x_1 + x_2 = c = 180^\circ - 2\alpha$ (1)

ΔABT_1: $x_1 + e = \alpha$ (2)

ΔDEG: $x_2 + r = \alpha + \beta$ (3)

$x_1 + x_2 + e + r = 2\alpha + \beta$

$e + r = (4\alpha - 180^\circ) + \beta$

$$\boxed{e + r = f + \beta} \quad (4)$$

This is the general law of internal double reflection. Angle $f = (4\ \alpha - 180^\circ)$ between incoming and outgoing ray, is constant for any stone with pavilion angle α. If x_1 or x_2 is larger than the opposite angle within the respective triangle, then, e or r are negative. Thus, e for ray AB and r for ray D_1E_1 are negative; e and r are inside ΔABT_1 and $D_1E_1T_2$, respectively. For rays AB_2 and DE, e and r are positive, while outside ΔAB_2T_1 and DEG. For table-to-table reflections, ray $A_1B_1D_1E_1$, $\beta = 0^\circ$.

facet at point D with an angle "x_2", and again reflected to the bezel facet, arriving at point E with an angle "r".

Section AB of the ray forms Δ ABT_1 with the table and the left pavilion facet. Section BD forms Δ BDC with the two pavilion facets, and section DE forms Δ DEG with the right pavilion facet and the crown facet. Each of the three triangles contains one of the design angles of the stone. A simple relationship between the entering and outgoing light ray and the design angles can be derived as shown in *Figure 3*, which leads to the general law of internal double reflection (IDR - law):

$$e + r = f + \beta$$

where $f = (4\alpha - 180^\circ)$ may be called the focus-angle of the stone.

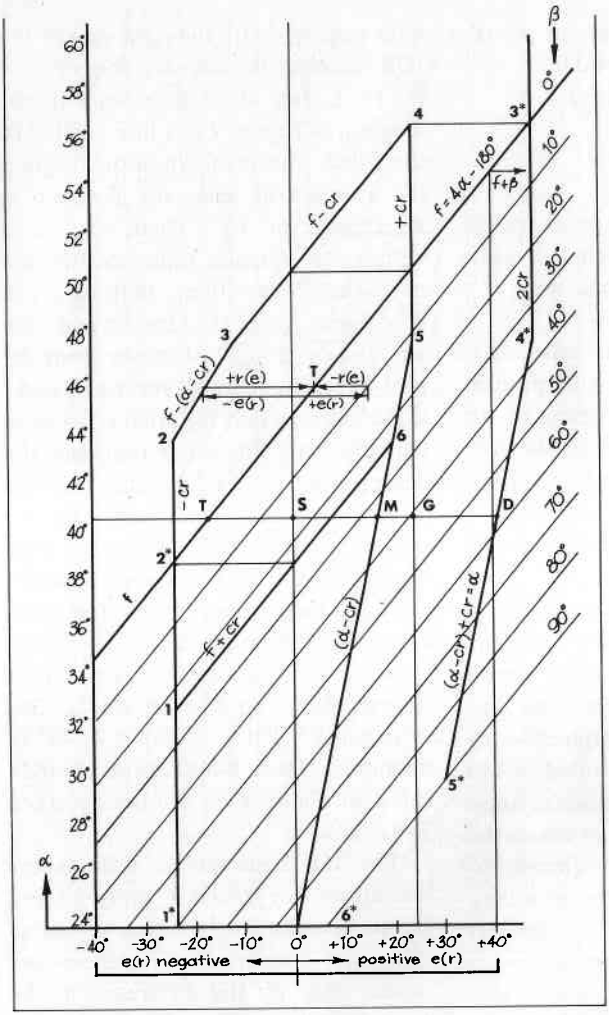

Fig. 4. Limits of double reflection in diamond. Table-to-table reflections are possible only, if angle e of the entering ray plus angle r of the outgoing ray fit the area framed by points 1 through 6. Frame 1 through 6* indicates the limitations of reflections through the crown facets (β – reflections).*

4. The Limitations of Internal Reflections

It has been pointed out in section 2 that angle "e" of the entering ray can vary between (+cr) and (–cr), so that e(max) = (+cr), and e(min) = (–cr). On the other hand, angle "x_1" (first reflection in *Figure 3)* cannot be smaller than cr for total reflection. According to *Figure 3*, $e + x_1 = \alpha$, or $e = \alpha - x_1$. Substituting cr for x_1 as the limit, we obtain e(max) = (α – cr). The difference (α – cr) increases with increasing α. However, it again cannot exceed cr. Thus, there are two limitations for e(max), depending on the size of α. It follows the angular margin of angle "e":

$$(-cr) \leqslant e \leqslant (\alpha - cr) \leqslant (+cr)$$

Substituting these limits for "e" in the IDR-equation, first for table-to-table reflections (β = 0°), so that e + r = f,

then we obtain the limitations for the outgoing angle "r" at the table:

limit (e)	limit (r)
+cr	f – cr
(α – cr)	f – (α – cr)
–cr	f + cr

These limitations are the basis for the diagram of *Figure 4,* which represents the conditions for diamond with cr = 24°.

The horizontal angular scale starts at the vertical zero-line with positive values of "e" or "r" increasing to the right, and negative values to the left. The critical angle is marked by vertical lines at (+cr) = (+24°) and (–cr) = (–24°). The pavilion angle α is scaled vertically.

The focus-angle f = (4α – 180°) is indicated by the inclined f-line, and the other 6 limitation terms appear accordingly in the diagram. This way the diagram becomes a graphical computer which is demonstrated as an example, for a cut with pavilion angle α = 46° in *Figure 4.* If a ray enters the table with an angle e = +15° (move 15° to the right, starting at the zero-line), then a move of r = –11° to the left (negative direction) leads to point f = 4° (design point for table reflections with α = 46°), so that the IDR-equation for table reflections, e + r = f, is satisfied. If e = –18° (move 18° from zero-line to the left), then r = +22°. The procedure is reversible, so that we can write: e(r) + r(e) = f; for e(r) read "e or r", and reverse.

Due to the limitations derived above, table reflections are possible only if the size of e and r is within the frame marked by points 1 through 6.

For reflections to the crown facet with angle $\beta > 0°$, the right side of the IDR-formula increases by β; e + r = f + β. Thus, any angle β appears in the diagram of *Figure 4* as a line parallel to the f-line. This is shown in the diagram by a series of lines for β-values in increments of 10°. Then, any point within the diagram indicates the size of α (horizontal line), that of β (inclined-line parallel f-line), and the amount of "f + β" (distance from the zero-line). The computation of e and r is the same as that for table reflections with the only difference that now the design point is "f + β" instead of "f".

Angle β, in general, can vary between 0° and 90°. However, since e(max) = (α – cr) $\leqslant$ +cr, and r(max) = +cr at the crown facet (compare *Figure 3),* the maximum of (f + β) = (α – cr) + cr = α or (f + β) = 2cr. It follows, β(max) = α – f = 180° – 3α, or β(max) = 2cr – f, (for $\alpha \geqslant 48°$ in diamond). These β-limitations are indicated in *Figure 4* by the lines marked 3*4*5*6*.

The IDR-equation as well as the limitations for e and r apply to any gemstone material. It is easy to recognize that numerical differences are caused only by the difference in the critical angles cr. This effect is demonstrated in *Figure 5* for zircon, corundum and quartz in comparison with diamond.

5. Interpretaion of The Reflection Diagram, *Figure 4*

The limitation for table-to-table reflections (frame 1 through 6) indicates that reflections through the table are possible for pavilion angles not larger than α = 57° and not smaller than α =

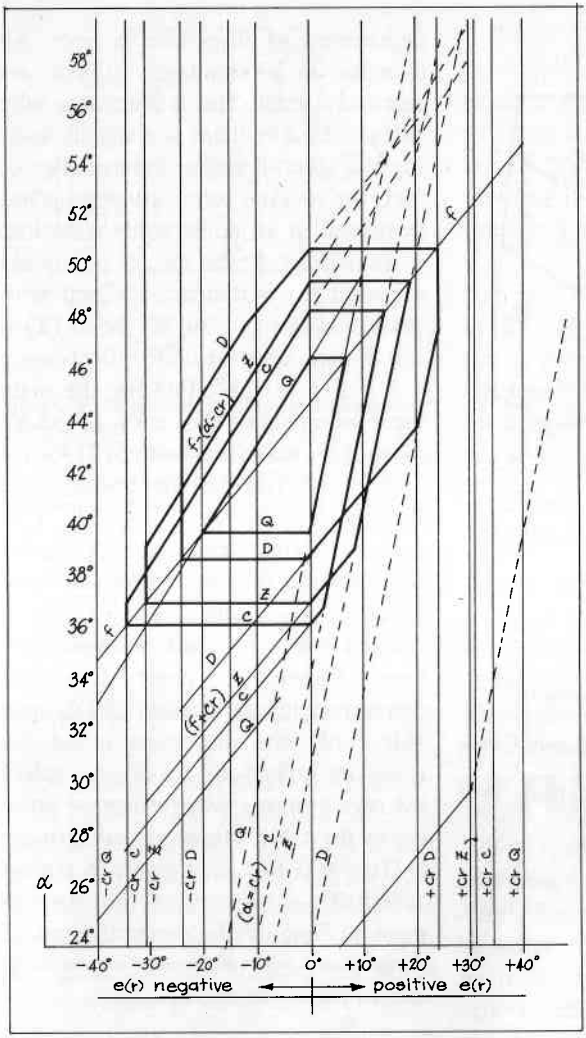

Fig. 5. Comparison of reflection limits in diamond, zircon, corundum, and quartz.
Symbols D, Z, C, Q refer to diamond, zircon, corundum, quartz, respectively.

33°. In these extreme cases, the interior of the stone viewed through the table appears "black." For a stone with $\alpha = 57°$, crown facets of any angle β also appear black, since $\beta(\max) = 2cr - f = 180° - 4\alpha + 2cr = 0°$. On the other hand, a stone with $\alpha = 33°$ gives crown facet reflections with β up to 81°; $\beta(\max) = \alpha - f = 180° - 3\alpha = 81°$.

The standard brilliant-cut diamond is equipped with 3 crown facets of different β-angles, the main facet (M) with β(M), the star facet (S) with β(S), and the upper girdle facet (G) with β(G). Facets β(M) and β(S) are responsible for the brilliance effect in connection with the table, while β(G) is designed primarily for dispersion.

Brilliance is the internal metallic

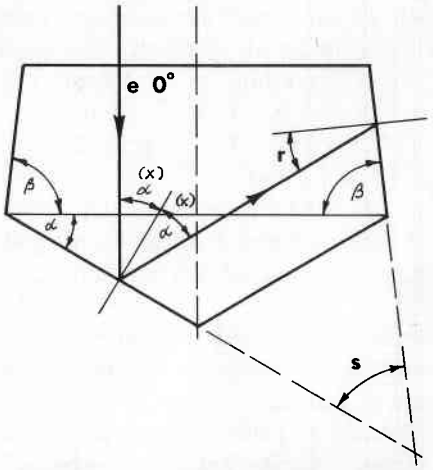

Figure 6. The principle of single reflection.
$e + x = \alpha$ *(see Fig. 3)*
$x = \alpha - e$
$x + r = s = \alpha - e + r$
$s = \beta - \alpha$
because,
$180° - \beta + \alpha + s = 180°$
It follows the law of single reflection:
$r - e = \beta - 2\alpha$
If $e = 0°$*, and* $r = cr$ *(for max. dispers.), then*
$\beta = 2\alpha + cr$
If $e = 0°$*, and* $r = 0°$ *(star facet effect), then*
$\beta = 2\alpha$

reflection of white light projected within a relatively small angular margin toward the observer. It is obtained from rays which enter the table at, or close to, 0°. These rays are of high intensity (see *Figure 2,* intensity scale), consequently, the bright shine of white light reflections.

Dispersion, as shown in *Figure 2,* is confined to rays which emerge grazing the facet. It occurs at all crown facets, even at the table. Due to the grazing departure, the direction of the spectral colors is almost identical with the angle β of the facet. If this angle is small, the projection of the spectrum is off the viewing direction, the perceptiveness of dispersion is poor. All β-angles in a standard brilliant are relatively small. This is the reason why the standard brilliant is allegedly lacking the spectral colors. As a matter of fact, the spectral colors are present but projected in an unfavorable direction.

In *Figure 4,* the design points are depicted for a standard brilliant with pavilion angle $\alpha = 40.8°$. Point (T) is the design point for table reflections, $e + r = f = -16.8°$, (M) for the main facet with $\beta(M) = (\alpha - cr) - f = 33.6°$, (S) for the star facet with $\beta(S) = -f = 16.8°$, and (G) for the upper girdle facet with $\beta(G) = cr - f = 40.8°$. This pattern defines entirely the angular proportions of this particular cut. None of the β-angles in this case is $\beta(max) = \alpha - f = 180° - 3\alpha = 57.2°$ (see *Figure 4,* point D). This $\beta(max)$-angle, designated $\beta(D)$, provides only the dispersion effect because its reflections are created solely by rays entering with $e(max) = (\alpha - cr)$ at the table. However, substituting β (D) for β (G) may result in a more acceptable angle combination for dispersion, because the perceptiveness of dispersion will increase appreciably due to the larger angle β (D).

6. Single Internal Reflections

The reflection diagram of *Figure 4* shows that the largest angle of $\beta = 90°$ corresponds with a pavilion angle $\alpha = 30°$. With such a pavilion angle, a ray vertically incident at the table, $e = 0°$, cannot be double-reflected by the two pavilion facets. The light path, after the first reflection, is parallel to the opposite pavilion facet as demon-

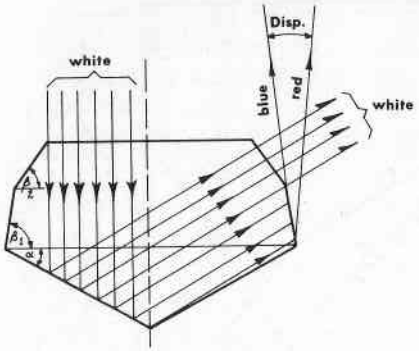

Figure 7. Suggested profile of a dispersion-cut diamond.
$\alpha = 29^\circ$; $\beta_1 = 2\alpha + cr = 82^\circ$; $\beta_2 = 2\alpha = 58^\circ$
Vertical incidence at the table causes max. dispersion of about 12° in observer direction at facet β_1. At facet β_2, vertically incident light emerges vertically to the facet. Since the light path is reciprocal, the table is completely lighted up, surrounded by a ring of spectral colors, followed by another ring of strong white light.

strated in *Figure 6.* Only single reflection takes place.

The formula for single reflection, $r - e = \beta - 2\alpha$, yields two distinct optical effects. If $e = 0^\circ$ (vertical incidence) and r = cr, so that $\beta = 2\alpha + cr$, high intensity dispersion will be obtained. With $e = 0^\circ$ and $r = 0^\circ$, thus, $\beta = 2\alpha$, a vertically incident ray at the table will depart from the facet of $\beta = 2\alpha$ vertically also. This effect resembles the star facet effect as discussed in the previous section.

In *Figure 7,* an approximate profile of such a design is depicted with a series of entering rays to show the alternate effect of dispersion and scintillation. The profile resembles an old-fashioned cut. It is primarily a dispersion-cut with a considerable loss of the total influx of light, though certainly quite interesting.

Angle α cannot be smaller than cr, i.e., α (min) = cr; otherwise a vertically incident ray would leak through the pavilion. On the other hand, r(max) = cr for dispersion, and the extreme limit of β is 90°. With these limitations, it follows from *Figure 6:* $\beta = 2\alpha + cr = 3\ cr = 90^\circ$. Thus, $cr = 30^\circ$ is the largest critical angle which allows a design like *Figure 7.* This corresponds to a refractive index of n = 2.0. Consequently, a dispersion-cut based on a single reflection is applicable to gemstone materials of $n \geqslant 2.0$ only.

7. Total Reflectivity, Brilliance and Perceptiveness of Dispersion

The total influx of light into a stone at any point of a crown facet cannot be more than 2 cr inside the stone. Since the pavilion facets are not ideal mirrors, reflection takes place only if the conditions for total reflection are satisfied, i.e., for those rays which impinge on a pavilion facet under an angle larger than cr. Due to this fact, the total reflectivity is always smaller than the total influx of light. The actual amount of total reflectivity for any pavilion angle α is readily obtainable from the diagram of *Figure 4.* The ratio between the total reflectivity and the total influx of light (2cr) indicates the percentage of reflectivity (R%) for any cut. Thus,

$$R\% = \frac{\text{total reflectivity}}{2cr} \cdot 100$$

The result is delineated for diamond in *Figure 8* and for comparison with other gemstones in *Figure 9.* It shows that for diamond, the reflectivity is largest, R = 91.5%, at a cut of pavilion angle $\alpha = 44^\circ$.

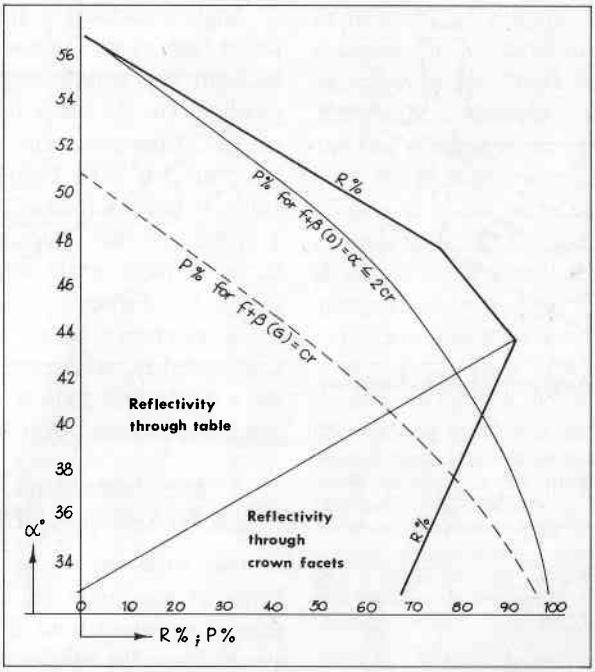

Figure 8. Percentage of reflectivity (R%) and perceptiveness of dispersion (P%) in diamond.

The total influx of light within one plane of incidence is equal to 2 cr. Reflectivity is possible for entering angles e between e(max) and e(min) which can be determined from Fig. 4 for any pavilion angle α. Then, the percentage of reflectivity is

$$R\% = 100 \cdot \frac{e(max) - e(min)}{2\,cr}$$

Dispersion is caused by rays, departing grazingly from the facet of angle β. The larger β, or the smaller (90° − β), the better are the dispersed rays projected toward the observer, thus, the better is the perceptiveness of dispersion. Analogous to Lambert's law of intensity, the perceptiveness may be expressed

$$P\% = 100 \cdot \cos(90^\circ - \beta) = 100 \cdot \sin\beta$$

The perceptiveness is plotted for f + β (G) = cr, and f + β (D) = (α ≤ 2 cr).

Here, the total reflectivity is equal to α, because, as discussed earlier, the total reflectivity is principally the difference between e(max) = (α – cr) and e(min) = (–cr) of the entering rays; thus, e(max) – e(min) = (α – cr) – (–cr) = α. This is true for all $\alpha \leqslant 44^\circ$. If $\alpha \geqslant 44^\circ$, the total reflectivity is reduced due to leakage at the second reflection (see *Figure 4*). On the other hand, table reflectivity for $\alpha \leqslant 44^\circ$ is smaller than the total reflectivity. This is indicated in *Figure 8* by the line which divides the area of total reflec-

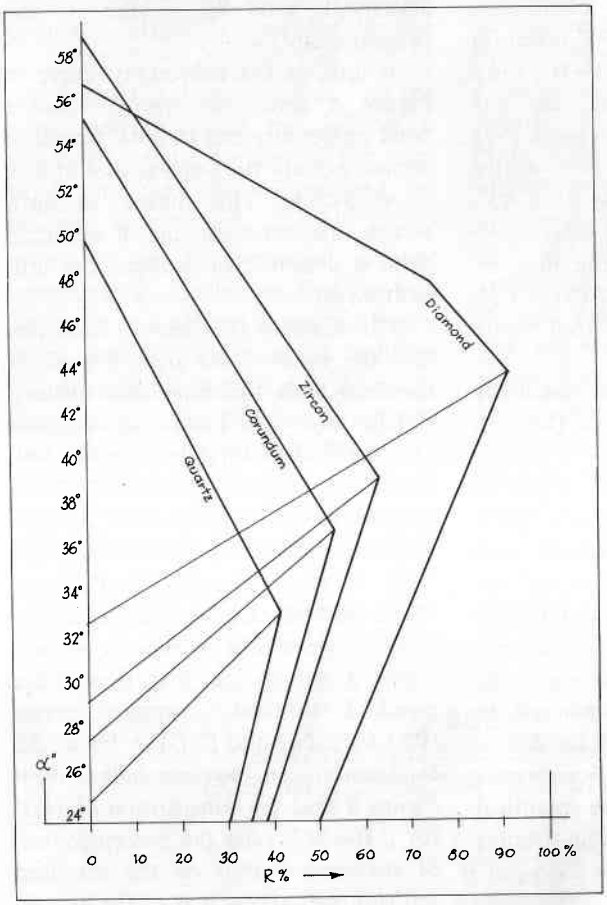

Figure 9. Reflectivities (R%) of diamond, zircon, corundum, and quartz.

tivity into two sections. The amount of total reflectivity is the prerequisite for brilliancy; however, both terms should not be considered identical.

The totally reflected light crosses the girdle plane again in a direction opposite to the entering direction. All of this back-reflected light (reflux) can escape through the crown facets, or only part of it, depending on the angle of the crown facets. If the total reflectivity is high (see *Figure 8)* and all the reflected light can go through the crown facets to the outside, the brilliancy of the stone will be a maximum. In this case only, total reflectivity and brilliancy are identical.

It can be shown that the reflux through facet (M) is an optimum, if a ray entering the table with e(max) = (α − cr) escapes through (M) with an angle r(min) = 0°. Then, f + β (M) = (α − cr), and β (M) = (α − cr) − f; table reflections and reflections through (M) supplement each other to the maximum of total reflectivity.

The star facets (S) in connection with the table, act like a 90°-prism (or $\alpha = 45°$-stone), if $f + \beta(S) = 0°$, and $\beta(S) = (-f)$. In this case, any ray entering the table with an angle (+e), departs facet (S) with (−r) = (−e), the same way as at the table of a 45°-stone. The full amount of total reflectivity is projected toward the observer. This condition of (S), $f + \beta(S) = 0°$, is possible only for $\alpha \leqslant 45°$ (see *Figure 4).*

The dispersion effect is essentially obtained from facets (G) and (D) with $\beta(G) = cr - f$, or $\beta(D) = \alpha - f$. Due to the grazing departure of dispersed rays, the spectral colors are increasingly perceptible by the observer with increasing β-angle. Thus, for the display of dispersion, $\beta(D)$ is preferable to $\beta(G)$. Based on this fact, the term "perceptiveness of dispersion" has been introduced and explained in *Figure 8.* The curves of P% are delineated for $\beta(G)$ and $\beta(D)$ with reference to pavilion angle α. The practical effect of dispersion perceptiveness may be recognized in *Figure 7.*

8. Comparison of the Standard Brilliant with "Historical Cuts"

In his article "Observations on Historical Shapes of Gem Diamond" *(Australian Gemmologist,* August, 73), H. Tillander, Helsinki, Finland, stated that in historical cuts "the angles of both the crown and the pavilion facets are 45° all the way around the girdle." He concludes, with particular reference to the standard brilliant, these cuts "are superior to modern stones both in brilliancy and dispersion." It is interesting to compare Tillander's statement with the results of the present study.

A look at the reflectivity curve in *Figure 8* reveals surprisingly that a total reflectivity of a ($\alpha = 45°$)-stone is almost exactly the same as that of a ($\alpha = 41°$)-stone. This means, in both stones, the same amount of reflected light is available to produce the brilliant effect.

The diagram of *Figure 4* indicates that the crown facet angle $\beta = 45°$ is identical with the dispersion angle β (D) for a ($\alpha = 45°$)-stone (intersection of $\alpha = 45°$-line with β-limit line 4*-5*). Thus, the dispersion facets (D) have been made the main facets of the ($\alpha = 45°$)-stone, while at the standard brilliant, the (G)-facets with $\beta(G)$ provide the dispersion. Due to this fact, the perceptiveness of dispersion is, indeed, higher at the 45°-cut than that of the standard brilliant (compare curves (P%) for $\beta(G)$ and $\beta(D)$ in *Figure 8).* It further can be concluded from *Figure 8* that the substitution of $\beta(D)$ for $\beta(G)$ will raise the perceptiveness of dispersion (P%) of the standard brilliant well above that of the historical 45°-stones.

On the other hand, star facets of the type suggested for the standard cut with $\beta(S) = (-f)$, which provide 100% of the total reflectivity, are not possible at the 45°-cut, because in this case, $f = 0°$, thus $\beta(S) = 0°$ (see *Figure 4).* Since the main facets of the 45°-cut are plain dispersion facets, the brilliance effect is confined to table reflections. These reflections, however, are strong because the pavilion acts like a 90°-prism where the direction of departing rays is parallel to that of the

entering rays. In the standard cut, the brilliance effect is provided by the table (T), the main facets (M), and the star facets (S). From the fact that the total reflectivity of the 45°-cut is practically equal to that of the standard, and that the brilliance of the 45°-cut is confined to table reflections, it can be estimated without complicated calculations that the brilliancy of the 45°-cut cannot be higher than that of the standard brilliant. Another interesting point in favor of a 40.8°-stone is the fact that in this case the total reflectivity (R%) and the perceptiveness of dispersion (P%) are equal and high (intersection of (R%)-curve with (P%)-curve for β (D) in *Figure 8).*

In addition to his enthusiasm for the ($\alpha = \beta = 45°$)-cut, H. Tillander emphasizes the "superb symmetry" of all historical cuts with reference to Vincent Peruzzi. This statement is in absolute agreement with all optical experience that symmetry provides the most accurate straight reflections of highest intensity within a plane of incidence, while deviations of a ray from the plane of incidence, due to asymmetric arrangements of the reflecting surfaces, decreases the intensity. From this point of view, it is not likely that recent suggestions to cut the pavilion with an uneven number of faces (asymmetry) will improve the optical quality of a brilliant-cut diamond.

The maximum dispersion is a discrete, invariable property of the gem material which is confined exclusively to grazingly departing light rays. Only

TABLE I
SUGGESTED DESIGN ANGLES FOR BRILLIANCE AND DISPERSION.

				Brilliance Scintillation			Dispersion			
Material	$\alpha°$	$(\alpha-cr)°$	$f°$	$\beta(M)°$ $=\alpha-cr-f$	$\beta(S)°$ $=(-f)$	R%	$\beta(G)°$ $=cr-f$	P%	$\beta(D)°$ $=-f$	P%
Diamond cr = 24°	45	21	0	21	0	87.5	24	40	45	71
	44	20	— 4	24	4	91.5	28	47	48	74
	43	19	— 8	27	8	89.5	32	53	51	78
	42	18	—12	30	12	87.5	36	59	54	81
	41	17	—16	33	16	85.5	40	64	57	84
	40	16	—20	36	20	83.3	44	69	60	87
Zircon cr = 31°	40	9	—20	29	20	61.5	51	78	60	87
	39	8	—24	32	24	63	55	82	63	89
	38	7	—28	35	28	60	59	86	66	91
Corundum cr = 34.5°	37	2.5	—32	34.5	32	54	66.5	92	69	93
	36	1.5	—36	37.5	36	52	70.5	94	72	95
Quartz cr = 40°	33	—7	—48	41	48	42	(88)	—	81	99

its direction toward the observer and its intensity can be changed by variation of the facet angles. Asymmetrical faceting can only weaken the over-all effect.

A variety of facet combinations which provide high brilliance and optimum dispersion are presented in *Table I* for diamond, zircon, corundum and quartz. In each case, the percentages of total reflectivity (R%) and of perceptiveness of dispersion (P%) are added.

9. Conclusion

The previous discussions have shown that the diagrams, especially of *Figures 4* and *8,* which are based on the inherent optical laws, are useful tools to design for special effects and to analyze the optical quality of faceted gemstones. The charts, worked out in detail for diamond, can easily be modified for any other gem material as discussed in Section 4. They indicate that the variety of the optical appearance of a faceted gemstone is practically unlimited. The preference for one or the other optical property of the gem material, such as brilliance and dispersion, or their gradual combination, is a matter of fashionable taste.

Diamond is known for its outstanding brilliance effect and dispersion, which are unique among all other natural gemstones. Cutting a diamond for "Colors" (dispersion) only, neglecting brilliance, seems to be a devious attempt to demonstrate the inherent beauty of this particular gem material, because spectral colors can be obtained even from glass (rhinestones), but not the quality of diamond brilliancy. Only by proportional cutting for brilliance and dispersion will the real beauty of a diamond come to light.

Developments and Highlights at GIA's Lab in Los Angeles

By RICHARD T. LIDDICOAT, JR.

Tesserae Mask

A large object brought in for an identification was one of the most unusual items we have ever been called on to identify. It was obviously the face portion of a human skull that had been covered by tesserae of what appeared to be turquoise. Two of the lower molars were still in the skull. The tesserae had bubbles and melted when a hot point was brought close. The material gave off a plastic odor. In other words, the skull was real and the tesserae were plastic. This seemed a

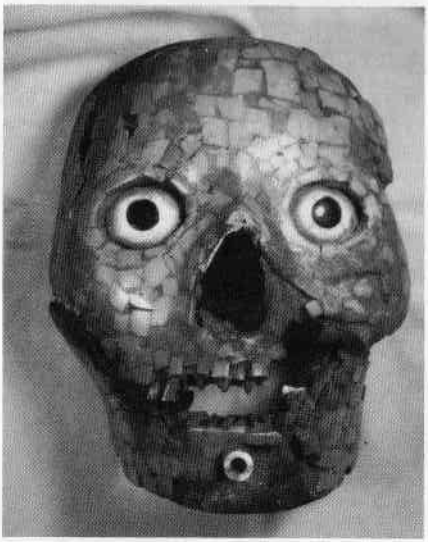

Figure 1.

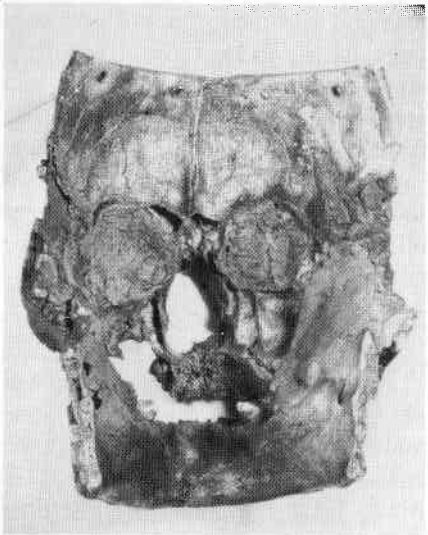

Figure 2.

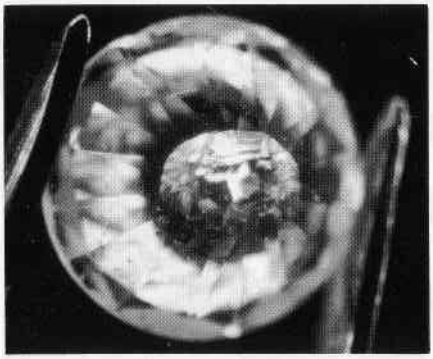

Figure 3.

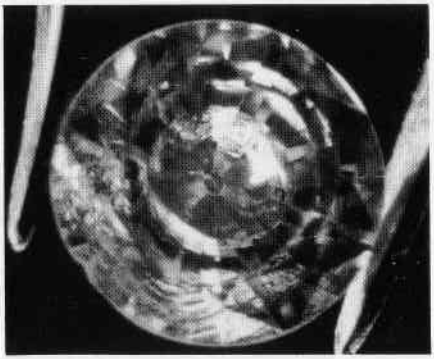

Figure 4.

strange combination. *Figure 1* shows the skull from the front and *Figure 2* from the back.

Interesting Inclusions in Diamonds and Resulting Appearances

In *Figure 3* we see a cleavage more or less parallel to, and rather near, the culet in the pavilion of a round brilliant cut diamond. Reflections exaggerate its extent, but obviously it is a very extensive cleavage. When this diamond is turned over and examined from above, *Figure 4,* the effect of the single cleavage is multiplied and appears to be seen all over the stone from a circular zone around the culet to several other series of circles. On the upper right-hand side, the cleavage reflections extend all the way to the girdle.

More Diamond Inclusions

Figure 5 is an excellent example of an "impossible" inclusion in a diamond. There is no way in which one could have imagined a situation in which diamond, crystallizing as it does at depths of over 100 kilometers below the surface, would have liquid and gas inclusions. This is a situation in which a cavity was open to the surface and water or another liquid was left in the cavity, together with a gas bubble. With even the gentlest heating, this cavity filling resembling an inclusion would have disappeared quickly. The photomicrograph was taken at 63x.

Other Odd Diamond Inclusions

In *Figure 6* we see a tubelike or needlelike inclusion in a diamond shown under 63x. When we double the magnification, we see that it has a

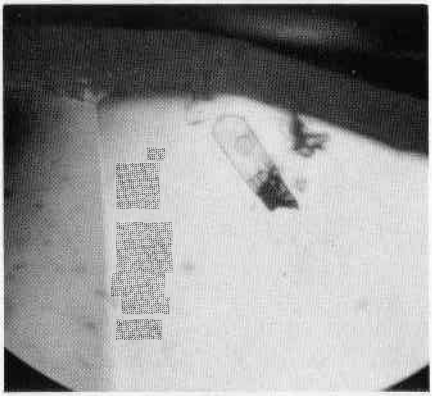

Figure 5.

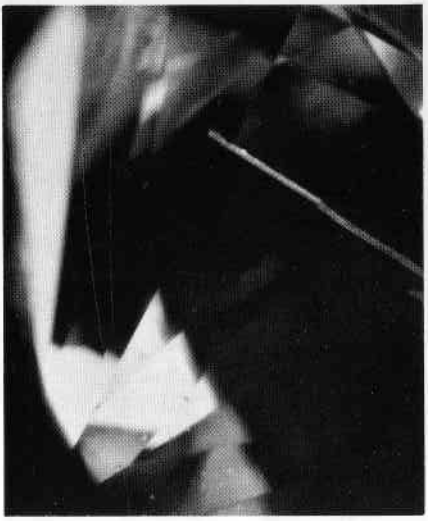

Figure 6.

Figure 7.

diamond-shaped cavity, seen in *Figure 7*. Unfortunately, the stone was not available for the time necessary for a detailed study.

Horsey Inclusion

The other diamond inclusion that was deemed worthy of recording was a perfect rendition of the bust of a horse. Karin Hurwit, Staff Gemologist, at the Los Angeles Laboratory, encountered this during the course of diamond grading activities. She is undecided whether it represents *Secretariat* or *The Trojan Horse.* It is shown at about 60x in *Figure 8.*

Opal Fakery

Figure 9 shows an opal doublet that was made to simulate boulder opal. The ironstone usually associated with the back portion of a boulder opal had been cemented to white opal that was quite transparent, giving the effect of a black boulder opal. It is shown at 10x in *Figure 9* and the separation between opal and ironstone is more evident at 63x in *Figure 10.*

Nephrite Horses

We received for identification a rather heavily banded and speckled gray-green statue of a mare feeding a young foal. In appearance, it resembled an aventurine or quartzite quartz,

Figure 8.

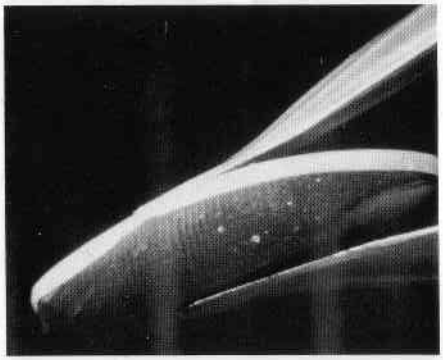

Figure 9.

Figure 10.

but the properties were those of nephrite. The odd appearance led us to scraping a bit from the stone and testing it by X-ray powder diffraction. The resulting diffraction pattern Chuck Fryer found was that of nephrite. It is shown in *Figure 11* at about one-third actual size.

Acknowledgements

We wish to express our sincere thanks for the following gifts:

To *Shonn Atkinson,* GIA Los Angeles Resident student, for a large collection of plastic beads simulating amber which will be put to good use in our resident gem identification classes.

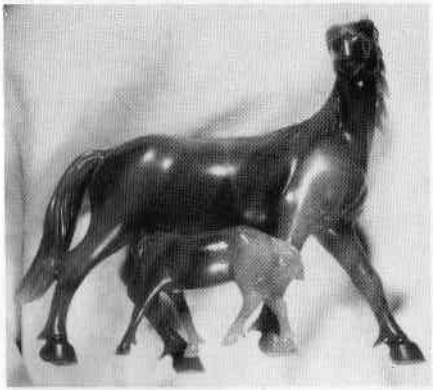

Figure 11.

To *H. T. Chen,* South China Company, Hong Kong, for an assortment of rough material which will be used in our gem identification classes.

To *Ben Gordon,* G.G., of Gordon Jewelry Corporation, Houston, Texas, for a grand assortment of natural and cut stones for our resident and correspondence course colored stone sets.

To *Kenneth and Phyllis Gunn,* GIA students from Spokane, Washington, for a much needed selection of 48 faceted natural sapphires from Montana to be used in our gem identification classes.

To *Richard B. Heckle,* C.G., of Claude S. Bennett, Inc., Atlanta, Georgia, for a large collection of miscellaneous cut stones including opals, natural sapphires, zircons, amethyst, citrine and smoky quartz.

To *George C. Houston,* R.S., of George C. Houston, Los Angeles, California, for a group of simulated crystal shapes cut from synthetic ruby for class use and our reference collection. Mr. Houston, our longtime benefactor of increasingly hard to find garnet-

and-glass doublets, gave GIA about 20,000 of them.

To *Donald Marchbank,* M.D., of Created Gem Imports, Salina, Kansas, for a generous donation of several specimens of the new Gilson "spider-web" pattern synthetic turquoise for our reference collection and colored stone class use.

To *Robert Miller,* G.G., and *Guy Paul,* G.G., of Friendship Gem Mining, Inc., of Los Angeles, California, for a varied assortment of polished and rough fire agates, gem gravels from Africa, and peridot from Arizona to be used in the resident gem identification course.

To *Tom Miller,* G.G., GIA Diamond Correspondence Course Instructor, Los Angeles, California, for an interesting 1.62 ct. oval faceted lazulite specimen for our reference collection.

To *Bob Nordbye,* GIA Correspondence student, Largo, Florida, for a well-faceted 8.9 ct. light green spodumene which will be exhibited in our display case. We wish to thank Bob for sharing this stone with us.

To *R. S. Peebles,* G.G., Minden, Nevada, for a collection of glass foil-backs to be used in our gem identification classes.

To *Arnold L. Reicherts,* of Aldo Jewelers, Inc., Boca Raton, Florida, for a fine round mix-cut blue natural sapphire with an unusual reddish inclusion for our gem identification class.

To *Laurie Skrivanek,* GIA Los Angeles Resident student, for an unusual "piggy-back" glass imitation diamond which will be used in the Resident Diamond course.

To *David L. Smith,* of Del Rio, Texas, for specimens of fire agate and malachite on quartz to be used in our gem identification classes.

To *Glenn Vargas,* dealer in rare and unusual gem materials, of Thermal, California, for numerous pieces of rough materials including prehnite, phosphophyllite, datolite, smithsonite, natrolite, rhodonite, sphene, brazilianite, and amblygonite, for our student testing sets.

On Gem Orthopyroxenes: Enstatite and Bronzite

BY PETE J. DUNN, M.A., F.G.A.
Department of Mineral Sciences
Smithsonian Institution
Washington, D.C. 20560

Introduction

Enstatite and hypersthene are members of an isomorphous series of orthorhombic pyroxenes. The pure end members of the series are enstatite, $MgSiO_3$ and orthoferrosilite, $Fe^{+2}SiO_3$. Iron and magnesium substitute mutually between $Mg_{100}Fe^{+2}{}_0$ and about $Mg_{10}Fe^{+2}{}_{90}$ (Deer *et al.*, 1963). Although petrologists have subdivided this series into 6 subspecies *(Table I)*, the practicing gemologist is primarily concerned with only the magnesium-rich members which yield some attractive gems. Adopting the classification used by Deer *et al.* (1963), enstatite is designated as a member of the series having 88% to

TABLE I
NOMENCLATURE OF THE ORTHOPYROXENES

enstatite	$En_{100}Fs_0$	to	$En_{88}Fs_{12}$	FeO < 6.50%
bronzite	$En_{88}Fs_{12}$	to	$En_{70}Fs_{30}$	FeO > 6.50%
hypersthene	$En_{70}Fs_{30}$	to	$En_{50}Fs_{50}$	FeO > 16.32%
ferrohypersthene	$En_{50}Fs_{50}$	to	$En_{30}Fs_{70}$	FeO > 27.23%
eolite	$En_{30}Fs_{70}$	to	$En_{12}Fs_{88}$	FeO > 38.12%
orthoferrosilite	$En_{12}Fs_{88}$	to	En_0Fs_{100}	FeO > 47.92%

En—Enstatite member
Fs—Orthoferrosilite member

100% of the magnesium end member; bronzite having 70% to 88% of the magnesium end member and hypersthene between 50% and 70% of the magnesium end member. Members of the series with Fe > Mg are usually opaque and of little gemological interest. It should be noted that meteoriticists use a slightly different classification wherein the enstatite-bronzite border is at 10% of the iron end member and the bronzite-hypersthene border is at 30% of the iron end member (Mason, 1962). Although this system aids in the classification of the chondrule meteorites, gem enstatites are best designated by the petrological classification in *Table I.*

The recent emergence, in the gem market, of a number of gem grade faceted "hypersthenes" prompted the author's investigation into this gem group. The present study of gem quality enstatite was initiated to determine the iron content, and hence the correct nomenclature, of these purported "hypersthenes," and gem enstatites in general.

Three faceted gems in the U.S. National Gem Collection, weighing 7.77, 8.07, and 10.93 carats each were examined. Eight other gemmy orthopyroxenes were also examined, including the Indian material originally noted by the American gemologist, John Sinkankas (1955), and donated by him to the Smithsonian Institution. Five samples from Brazil were donated by Miss Tomiko Butler, F.G.A. of Silver Spring, Maryland, U.S.A., who generously and thoughtfully donated fragments of the rough for this study before cutting the gems. Other occurrences include the noted Ceylon greenish enstatite, and the dark green material from the San Carlos Indian Reservation in Arizona (Sinkankas, 1959).

All numbered specimens are from the U.S. National Mineral Collection at the Smithsonian Institution, Washington, D.C. 20560. Specimens with numbers prefixed by "G" are faceted gems on exhibit.

Previous Work

For discussions of asterism and inclusions in star enstatite, the reader is referred to the work of Eppler (1967) and (1971). Early work on gem enstatite was done by Mitchell (1953) (1954) and Trumper (1954). Tanzanian enstatite was recently noted by Bank (1974).

Chemistry

All the samples were analyzed on an ARL-SEMQ electron microprobe utilizing an operating voltage of 15KV and a sample current of 0.15Mu. Wet-chemically analyzed enstatite and hypersthene microprobe standards of high reliability were used. The analyses are presented as *Table II,* in order of increasing iron content, together with their densities, color, and localities.

The examined gems are all magnesium-rich with the FeO content varying from 2% to 11% by weight. It is quite obvious that gem enstatites and bronzites vary little in composition for a given locality. None of the samples, including six offered for sale as hypersthene, contained sufficient iron to be considered hypersthene. The Tanzanian enstatites were the purest of those examined and the Ceylon gems next in relative purity.

TABLE II. ANALYSES OF GEM ORTHOPYROXENES

	NMNH	SiO_2	Al_2O_3	FeO	MgO	MnO	CaO	K_2O	Na_2O	TiO_2	Total	D	Locality	Color	Percent Enstatite End-Member
ENSTATITE	G-5459	58.79	1.33	1.89	38.29	0.08	0.08	0.00	0.05	0.03	100.54	3.25	Tanzania	Brown	95
ENSTATITE	126031	59.55	1.33	2.00	37.78	0.09	0.06	0.00	0.04	0.02	100.87	3.24	Tanzania	Brown	94
ENSTATITE	G-2294	58.04	0.78	5.17	35.26	0.16	0.53	0.02	0.02	0.03	100.01	3.31	Ceylon	Brownish green	88
ENSTATITE	G-3638	58.24	0.84	5.23	35.44	0.15	0.51	0.03	0.03	0.01	100.48	3.31	Ceylon	Brownish green	88
ENSTATITE	134302	56.60	3.27	5.67	33.68	0.15	1.10	0.00	0.07	0.14	100.68	3.31	Arizona	Dark green	84
ENSTATITE	134309	56.28	3.18	5.77	33.24	0.16	0.83	0.01	0.09	0.06	99.62	3.32	Arizona	Dark green	83
BRONZITE	134303	56.23	3.51	6.80	33.17	0.14	0.99	0.00	0.15	0.20	101.19	3.32	Arizona	Dark green	83
BRONZITE	BUTLER	57.01	0.53	8.97	33.50	0.20	0.22	0.01	0.02	0.03	100.49	3.32	Brazil	Brown	84
BRONZITE	134001	55.93	0.63	9.78	31.91	0.24	0.26	0.00	0.03	0.03	98.81	3.34	India	Greenish brown	79
BRONZITE	134002	58.03	0.60	10.02	32.53	0.24	0.25	0.01	0.03	0.04	101.75	3.32	India	Brown	81
BRONZITE	BUTLER	56.99	0.54	10.43	32.45	0.20	0.24	0.00	0.02	0.02	100.89	3.32	Brazil	Brown	80
BRONZITE	BUTLER	56.45	0.62	10.50	32.33	0.20	0.24	0.02	0.02	0.00	100.38	3.32	Brazil	Brown	80
BRONZITE	BUTLER	57.01	0.56	10.73	32.47	0.22	0.25	0.01	0.03	0.01	101.29	3.32	Brazil	Brown	80
BRONZITE	BUTLER	56.15	0.65	10.77	32.12	0.25	0.27	0.03	0.02	0.03	100.29	3.32	Brazil	Brown	80
BRONZITE	134003	57.35	0.55	11.08	32.32	0.25	0.26	0.01	0.03	0.05	101.90	3.35	India	Brown	80

Although the density of the orthopyroxenes varies from 3.21 to 3.95, the densities of the gemmy enstatites and bronzites examined in this study varied from 3.24 to 3.35. Gems with high iron content have the higher densities. Members of this series with densities less than 3.30 may be considered enstatite, and those with densities between 3.30 and 3.44 may be designated as bronzite.

Optical Properties

The refractive indices of the orthopyroxenes have been studied in great detail and several excellent graphs relating the optical constants to composition have been prepared (Deer *et al.*, 1963).

The indices and birefringence increase with increasing iron content. Values for gemmy enstatites and bronzites vary as follows: α = 1.650–1.665, β = 1.655–1.676, and γ = 1.665–1.690. Birefringence values vary from 0.015 to 0.025. The optic sign changes from positive to negative at about $En_{88}Fs_{12}$. This change in optic sign was taken as the demarcation point between enstatite and bronzite and may be used with reliability in determining the correct designation for a gem.

The color of enstatite and bronzite is not related to the FeO content; both the low-iron Tanzanian enstatite, the relatively high-iron Indian bronzite, and the Brazilian bronzite are a medium brown color.

Pleochroism in orthopyroxenes has not been explained in terms of chemical composition. Several investigators (Howie, 1955; Parras, 1958) have suggested that the pleochroism might be due to oriented intergrowths of diopside lamellae but no such lamellae were observed in the visible pleochroic Tanzanian and Ceylon enstatites. Although rock-forming enstatites are not usually pleochroic, the Tanzanian enstatites exhibit very strong pleochroism and the Ceylon enstatites moderate to weak pleochroism. The bronzite from India also exhibited strong pleochroism.

Optical data for the enstatite from Tanzania (G-5459), the one nearest to the enstatite end of the series, is given

as *Table III.* None of the examined gems were luminescent in either long or short-wave ultraviolet or in CuKα x-radiation.

Enstatite occurs as prismatic crystals, with a blocky habit. The rough is ideally suited to emerald and rectangular cuts. The gems are usually oriented with the table parallel to $\{100\}$ to obtain maximum yield, and sometimes with a table parallel to $\{010\}$ as these directions provide the most pleasing color. This preferred orientation in cutting aids the gemologist for gems with tables cut parallel to $\{100\}$ permit the direct measurement of true α and β and gems with tables parallel to $\{010\}$ will permit the measurement of true β and γ.

An interference figure, with $2V = 90^\circ$ is a helpful determination as it indicates that the gem's composition lies on the enstatite-bronzite border. This is only applicable in the case of a gem with a density between 3.25 and 3.35 as 2V also approaches 90° at the eulyite-orthoferrosilite border in the iron-rich end of the series.

Absorption Spectra

Although enstatites are known to always have a strong absorption line at 5060 Å, other spectral lines were observed and recorded. All samples exhibited the 5060 Å line, and it was the dominant line in each case. In addition to this dominant line, Tanzanian gems also had diffuse lines at 4550, 4880 and 5550 Å, Ceylon gems had one diffuse line at 5550 Å, Indian and Brazilian material had diffuse lines at 4880 and 5550 Å, and Arizona, U.S.A., gems had one diffuse line at 4880 Å.

TABLE III
OPTICAL DATA FOR TANZANIA ENSTATITE
($En_{95}Fs_5$)

α = 1.653 (±0.002) Optic sign +
β = 1.655 (±0.002) Birefringence 0.010
γ = 1.663 (±0.002)

PLEOCHROISM

X =	*b*	Light brown
Y =	*a*	Brown
Z =	*c*	Green

Although an uncommon gem material, and one whose low hardness (5½ - 6) and perfect easy cleavage in two directions restrict its use in jewelry, enstatite and bronzite do provide very attractive gems. This material is also quite useful in teaching gemology inasmuch as it is a biaxial gem mineral with noticeable pleochroism; a material in which the optical constants and optic sign determination can provide a correct nomenclature designation, and one in which correct orientation is essential to the lapidary.

Inclusions in the studied enstatites were uncommon. Several of the Arizona bronzites had exsolution lamellae of diopside. Inclusions in the Tanzanian enstatite will be the subject of a subsequent investigation.

The author is indebted to Ms. Tomiko Butler for thoughtfully providing the Brazilian gem bronzites, and to Dr. George Switzer for a critical reading of the manuscript. Mr. John Sinkankas and Mr. & Mrs. Clayton Macy generously provided the samples from the San Carlos Indian Reservation in Arizona, U.S.A. Additional

thanks also goes to Miss Ann Garlington for keeping the office candy jar full.

References

Bank, H. (1974) Durchsichtige grune enstatite aus Tansania 2. Dt. Gemmol. Ges. **23**, #3, 192-194.

Deer, W.A., Howie, R. A., Zussman, J. (1963) *Rock Forming Minerals* Vol. 2, Chain Silicates 8-41.

Eppler, W.F. (1967) Star Diopside and Star Enstatite, *Journ. Gemm.* **10**, 185-188.

Eppler, W.F. (1971) Some Rare Materials. *Journ. Gemm.* **12**, #7, 256.

Howie, R.A. (1955) The Geochemistry of the Charnockite Series of Madras, India. *Trans. Roy. Soc. Edin.* **62**, 725.

Mason, B. (1962) *Meteorites,* P. 62. John Wiley & Sons, New York.

Mitchell, R. K. (1953) A New Variety of Gem Enstatite. *The Gemmologist* XXII, #265, 145.

Mitchell, R. K. (1954) Some Further Notes on Hypersthene-enstatite. *The Gemmologist,* XXIII #280, 195-196.

Mitchell, R. K. (1954) Some Notes on Unusual Gems. *Journ. Gemm.,* **4** #5, 211.

Parras, K. (1958) On the Charnockites in the Light of a Highly Metamorphic Rock Complex in South-Western Finland. *Bull. Comm. Geol. Finland* #181,1.

Sinkankas, J. (1955) Some Freaks and Rarities Among Gemstones: Enstatite-Hypersthene from India. *Gems & Gemology,* 8, #6, 197-202.

Sinkansas, J. (1959) *Gemstones of North America,* 434-436. Van Nostrand Reinhold.

Trumper, L. C. (1954) Distinguishing Kornerupine from Enstatite. *The Gemmologist* XXIII, #276, 125-127.

Developments and Highlights at GIA's Lab in New York

By ROBERT CROWNINGSHIELD

More Diamond Inclusions

The owner of the diamond shown in *Figure 1* had submitted the stone for possible flawless grading. It was an unusual insect-like cloud that prevented any thought of a flawless stone. In addition to the "insect" a series of the following pinpoints suggests an aerial egg-layer.

In *Figure 2* we see two beautifully formed octahedral inclusions in an otherwise clear diamond. Not shown in the photograph are trigons present on the faces of the larger crystal.

We are pleased to add to our collection of diamonds with interesting inclusions the rough specimen shown in *Figure 3* received through

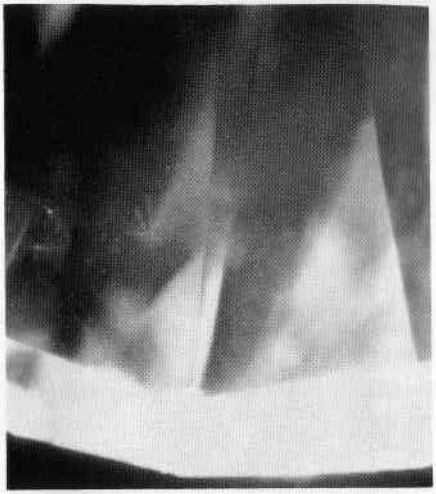

Figure 1.

Figure 2.

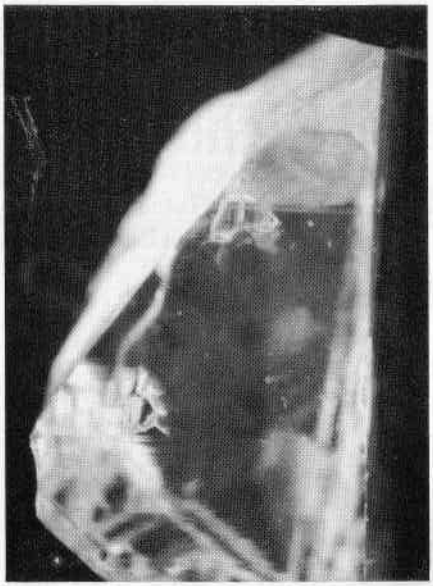

Figure 3.

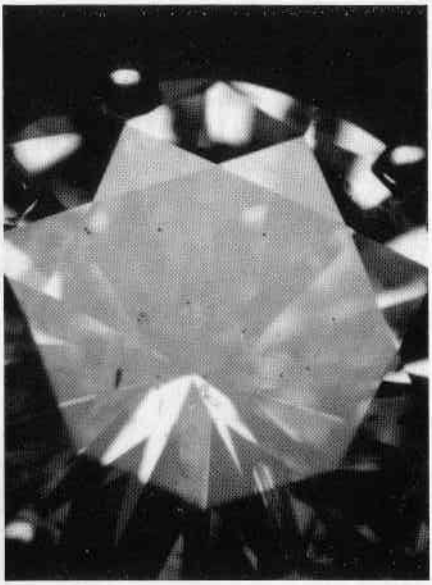

Figure 4.

the good offices of Mr. George Kaplan, Lazare Kaplan and Sons. The smaller inclusion to the left is transparent green and the sawing operation has exposed it to the surface. It is possible to read a doubly refractive index in the vicinity of 1.66. The larger inclusion is yellow brown in color and also transparent. A study of the superb photos in Dr. Gübelin's *Internal World of Gemstones* suggests that the green inclusion may be chrome enstatite or chrome diopside and the yellowish-brown crystal a garnet.

While the three diamonds described above have inherent inclusions, the 2.50-carat round brilliant shown in *Figure 4* has 17 inclusions that nature never intended. Not all 17 of the laser drillholes in the table of this stone can be seen in the photograph, although 12 can be. Viewed from the pavilion the stone appears to be crackled with inclusions, since by reflection each drill hole is doubled as are the inclusions which prompted the drilling to begin with.

A Painted Blue Diamond

The blue diamond tester or conductometer manufactured by the Institute came in very handy recently when a large grey-blue round brilliant in a ring came in for testing. The color was typical of many Type IIb diamonds and it should have conducted electrical current. However, it did not, and moreover it showed a distict "Cape" absorption spectrum in the hand spectroscope. Now we studied the stone under the microscope and, using both overhead and transmitted dark-field illumination, we were able to detect a skillfully applied coating—too subtle

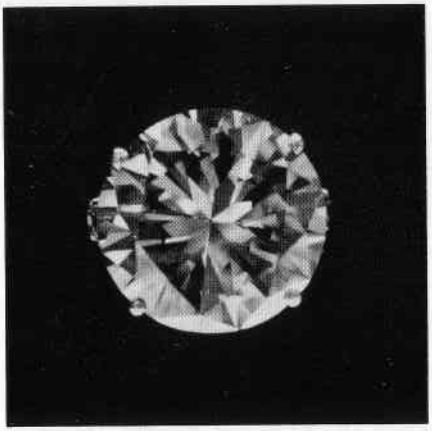

Figure 5.

to photograph. The well cut stone, however, is shown in *Figure 5*.

GGG

Now that the jewelry trade has been advised that Gadolinium Gallium Oxide (the garnet structured synthetic) is perhaps the most convincing diamond imitation yet to come on the market, we are beginning to see it come in for testing. One faint yellow stone (approximately "M" on the GIA Color Grading Scale) was a new color to us and a real fooler. Usually the color tends to be brownish with some stones tending to become darker brown upon exposure to ultra-violet. We have already heard of a case in which GGG was involved in a $1500 swindle. It is clear from the photos in *Figure 6* and *7* that the setter assumed that he was setting a diamond in a man's gypsy ring. In *Figure 6* we can see deep abrasions from either an automatic hammer or burnishing tool made before the stone broke completely under the treatment.

Figure 6.

Figure 7.

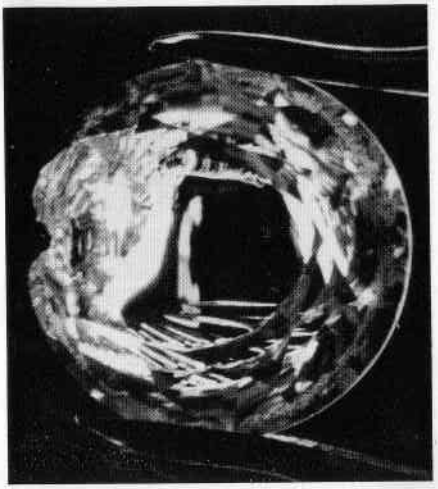

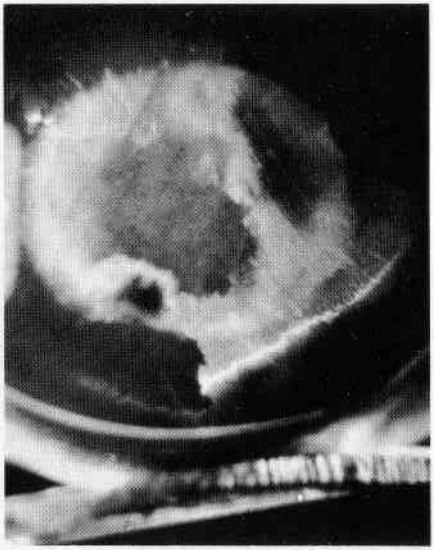

Figure 8.

Synthetic Opal

Since Mr. Pierre Gilson first introduced his black synthetic opal several years ago, we have seen several variations in appearance and properties. The most recent to come our way have shown distinct hexagonal patches within the individual larger color areas with characteristic black spots. These are much easier to detect as synthetic stones although their great beauty is still "too good to be true." One stone tested recently became permanently discolored following a refractive index reading. The dull gray spot is shown in *Figure 8*. The stone was evidently very porous suggesting that if placed on the tongue it would adhere—as many Mexican opals will do. It did adhere and turned an ugly brown temporarily until all the moisture had evaporated. Obviously, the run from which this stone came would not be satisfactory in jewelry.

Flux Grown Synthetic Rubies

Since the last issue of *Gems & Gemology* we have been asked to test a number of synthetic rubies which proved to be very good simulants of the real item. One cabochon shown in *Figures 9* and *10* displayed the typical bluish band and the seed crystal. It was very dark red in color resembling

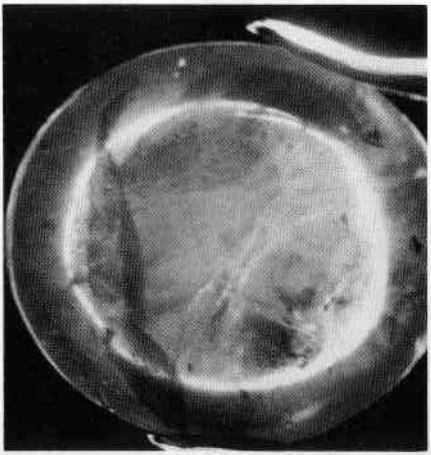

Figure 9.

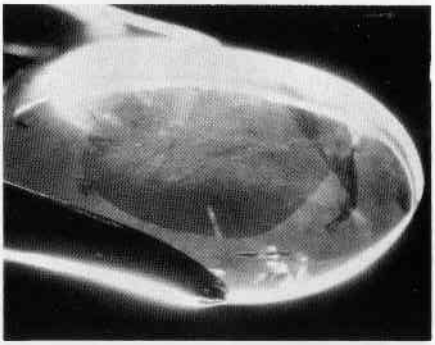

Figure 10.

some African natural stones. One flux-grown synthetic had been put into an old platinum lady's cluster ring. The jeweler was not too careful, since he had broken the tips of several prongs, but may have accomplished his nefarious aim of swindling an unwary buyer.

Acknowledgements

We wish to express our sincere thanks for the following gifts and courtesies:

To *Mr. Bill Larsen* and his charming wife *Karla* and his staff for a late afternoon reception at *The Collector Shop* in Fallbrook, California. Bill had prepared a very welcome selection of crystals from all over the world including a cube of boleite, the mineral featured on the cover of a recent *Lapidary Journal* issue. With crocoite, axinite, wulfenite, scorodite, cuprite, anglesite, in addition to more common minerals, one can see the range and interest of this gift. An unusual cut stone and rough from which it came is shown in *Figure 11.* It is a very clean but misty cabochon of hessonite garnet.

To *Mrs. Charles J. Mann,* Manhattan Beach, California, for a carved Corozo nut which resembles a fat Brazil nut and which the writer recalls seeing in his aunt's curio cabinet 40 years ago. *Figure 12* shows the hard "ivory" forming the face and the husk forming the headdress. Robert Webster in his book *Gems* has a good discussion of this rarely encountered gem material.

To *Mr. Irving Michaels* of Michaels Jewelers, Connecticut, for a beautifully varied selection of oval garnets from East Africa. They will be useful for both regular testing work in classes as well as for study in the new Colored Stone Appreciation Class being readied by Cap Beesley.

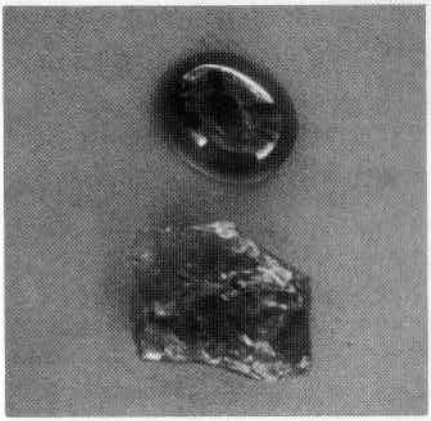

Figure 11.

Figure 12.

In Memoriam

CARLETON G. BROER

Carleton G. Broer, Vice Chairman and long time Governor of the Gemological Institute of America, died on December 21, 1975.

Cog Broer became a Certified Gemologist in 1939 and was one of the better known gemologists in the United States. He was twice President of the American Gem Society: from 1942 to 1943 and again from 1946 to 1948. In 1969 he was the first recipient of the Robert M. Shipley Award for his immeasurably valuable contributions to the American Gem Society. In addition, he served as Treasurer and as a member of the Executive Committee of the Retail Jewelers of America.

Broer graduated from Dartmouth in 1927 and many years later received the Alumni Award for his unfailing assistance to the college. He was an exceptionally effective fund raiser for Dartmouth and for his church. He served for many years as President of Broer-Freeman of Toledo, Ohio, a firm founded in 1877 by his father.

Coggie Broer was one of the most intelligent and logical men to grace the gemological firmament. In a meeting, he always could be depended upon to suggest a logical solution to a critical problem, the answer to which had eluded the majority of people in attendance. His effectiveness was indelibly impressed on every person who had the privilege of working with him. He was one of the truly remarkable men the gemological and jewelry fields have been fortunate enough to know.

Carleton Broer is survived by his widow Susanne, his son Carleton, Jr., better known as Tony, and two daughters, Linda Broer and Carole, now Mrs. Robert R. Bishop, Jr.